Side Chain Mobility and Ligand Interactions of the G Strand of Tear Lipocalins by Site-Directed Spin Labeling†

B. J. Glasgow,*,‡,§ O. K. Gasymov,‡ A. R. Abduragimov,§ T. N. Yusifov,‡ C. Altenbach,§ and W. L. Hubbell§,||

Departments of Pathology, Ophthalmology, and Chemistry & Biochemistry, University of California at Los Angeles School of Medicine, Los Angeles, California 90095

Received June 11, 1999; Revised Manuscript Received August 20, 1999

ABSTRACT: Side chain mobility, accessibility, and backbone motion were studied by site-directed spin labeling of sequential cysteine mutants of the G strand in tear lipocalins (TL). A nitroxide scan between residues 98 and 105 revealed the alternating periodicity of mobility and accessibility to NiEDDA and oxygen, characteristic of a β-strand. Residue 99 was the most inaccessible to NiEDDA and oxygen. EPR spectra with the fast relaxing agent, $K_3Fe(CN)_6$, exhibited two nitroxide populations for most residues. The motionally constrained population was relatively less accessible to $K_3Fe(CN)_6$ because of dynamic tertiary contact, probably with side chain residues of adjacent strands. With increasing concentrations of sucrose, the spectral contribution of the immobile component was greater, indicating a larger population with tertiary contact. Increased concentrations of sucrose also resulted in a restriction of mobility of spin-labeled fatty acids which were bound within the TL cavity. The data suggest that sucrose enhanced ligand affinity by slowing the backbone motion of the lipocalin. The correlation time of an MTSL derivative (**I**) attached to F99C resulted in the lack of side chain motion and therefore reflects the overall rotation of the TL complex. The correlation time of F99C in tears (13.5 ns) was the same as that in buffer and indicates that TL exists as a dimer under native conditions. TL−spin-labeled ligand complexes have a shorter correlation time than the protein alone, indicating that the fatty acids are not rigidly anchored in the cavity, but move within the pocket. This segmental motion of the ligand was modulated by protein backbone fluctuations. Accessibility studies with oxygen and NiEDDA were performed to determine the orientation and depth of a series of fatty acid derivatives in the cavity of TL. Fatty acids are oriented with the hydrocarbon tail buried in the cavity and the carboxyl group oriented toward the mouth. In general, the mobility of the nitroxide varied according to position such that nitroxides near the mouth had greater mobility than those located deep in the cavity. Nitroxides positioned up to 16 carbon units from the hydrocarbon tail of the ligand are motionally restricted and inaccessible, indicating the cavity extends to at least this depth. EPR spectra obtained with and without sucrose showed that the intracavitary position of lauric acid in TL is similar to that in β-lactoglobulin. However, unlike β-lactoglobulin, TL binds 16-doxyl stearic acid, suggesting less steric hindrance and greater promiscuity for TL.

Lipocalins function mainly to transport small hydrophobic molecules (*1*). X-ray crystallography and computer-generated models of several lipocalins have revealed common structural features (*2*−*8*). The calyx of the lipocalins is formed by eight antiparallel strands joined by loops (*2*). Many of the lipocalins, including major urinary protein, bilin-binding protein, pregnancy protein 14, β-lactoglobulin, and odorant binding protein, have been purified as dimers (*2*).

In the lipocalins that have been crystallized in the bound state, the ligand is almost invariably observed to bind inside the β-barrel. Data for β-lactoglobulin suggest that fatty acids may bind externally (*9*). However, in crystals of β-lactoglobulin−ligand complexes, lauric and palmitic acid lie within the cavity. The carboxyl group of the fatty acids is bound to Lys at the mouth of the cavity, and the hydrophobic tail is stretched to the calyx center (*7*, *8*).

Lipocalins are functionally diverse, which can be attributed in part to the varied specificity of the molecules they carry. Retinol binding protein is restricted to the transport of mainly retinol derivatives (*2*). Other lipocalins, such as β-lactoglobulin, have a much broader specificity. The structural features that confer specificity of binding have not been fully elucidated, but cavity size and backbone flexibility may be important. The lipocalins have a low degree of primary sequence homology (∼20%) but retain three conserved regions on the A, F−G, and H strands (*2*). The tryptophan of the A strand is invariably conserved in all of the lipocalins. The G strand has been implicated in the binding site because residues in this strand are close to ligands (*3*, *10*, *11*). In addition, many lipocalins exhibit a conserved disulfide bond usually linking cysteines in the D strand to one near the carboxy terminus (*1*, *2*).

† This work was supported by U.S. Public Health Service Grants EY11224, EY05216, and EY 00331, an unrestricted grant from Research to Prevent Blindness (B.J.G.), the Karl Kirchgessner Fund (B.J.G.), the Bundy Foundation (B.J.G. and W.L.H.), and the Jules Stein Professorship (W.L.H.).

* To whom correspondence should be addressed: 100 Stein Plaza, Rm B279, Los Angeles, CA 90095. Phone: (310) 825-6998. E-mail: bglasgow@pathology.medsch.ucla.edu.

‡ Department of Pathology.

§ Department of Ophthalmology.

|| Department of Chemistry & Biochemistry.

10.1021/bi9913449 CCC: $18.00
Published on Web 09/24/1999

Tear lipocalins (TL)[1] comprise 15−33% of the protein content of tears and are the principal lipid binding proteins in tears (*12*, *13*). TL are promiscuous binders of a broad range of lipids, including fatty acids, glycolipids, phospholipids, and cholesterol in tears (*12*).

An intact disulfide bond diminishes the affinity of TL for retinol and restricts the displacement of native ligands by retinol (*14*). The conserved tryptophan 17 on the A strand is the only tryptophan in TL (*6*). Changes monitored by fluorescence and near-UV CD spectroscopy reveal alteration in the environment of the tryptophan with ligand binding (*15*). Using site-directed tryptophan fluorescence, we previously identified the putative G strand of TL, resolved alternating periodicity in amino acid residue exposure characteristic of β structure, and determined the strand orientation as well as the relative depths of residues in the cavity (*16*). Here we sought to establish through EPR, dynamic changes in the G strand, including side chain mobility, tertiary contact with residues from other strands, and backbone motion. Further, we report the ligand orientation in the cavity and the influence of backbone motion on ligand binding.

EXPERIMENTAL PROCEDURES

Materials. MTSL was obtained from Toronto Research Chemicals, Inc. (Toronto, ON). A derivative of MTSL (**I**, Figure 1) was a generous gift from K. Hideg. The nitroxide derivatives of lauric acid and palmitic acid, C-12 and C-16 spin-labels (Figure 1), respectively, were synthesized according to previous methods (*17*). 5dxSA, 16dxSA, and β-lactoglobin were obtained from Sigma (St. Louis, MO). All reagents and solvents were analytical grade or better. *Escherichia coli* BL21(DE3) cells and pET 20b were obtained from Novagene. Oligonucleotide primers were obtained from Universal DNA, Inc. PCR II was obtained from Invitrogen (San Diego, CA). HiTrap columns were obtained from Pharmacia Biotech Inc. (Piscataway, NJ). Gas-permeable TPX capillaries were obtained from Wilmad Glass Co. Inc. (Buena, NJ). TL and apo-TL were obtained as previously described (*14*).

Site-Directed Mutagenesis and Plasmid Construction. The tear lipocalin cDNA in PCR II previously synthesized (*18*) was used as a template to clone the TL gene spanning bases 115−592 of the previously published sequence (*6*) into pET 20b with flanking restriction sites for *Nde*I and *Bam*HI as previously described (*16*). In addition to the wild type that contained cysteine at 101, we prepared three tear lipocalin mutants with cysteine 101 substitutions, C101A, C101L, and C101S, by the introduction of a point mutation by sequential PCR steps (*16*). C101L (WTT) was chosen as the template for additional mutant cDNAs because it exhibited structural features and binding characteristics similar to those of spin-labeled lipids (see the Results and Discussion). Ten additional

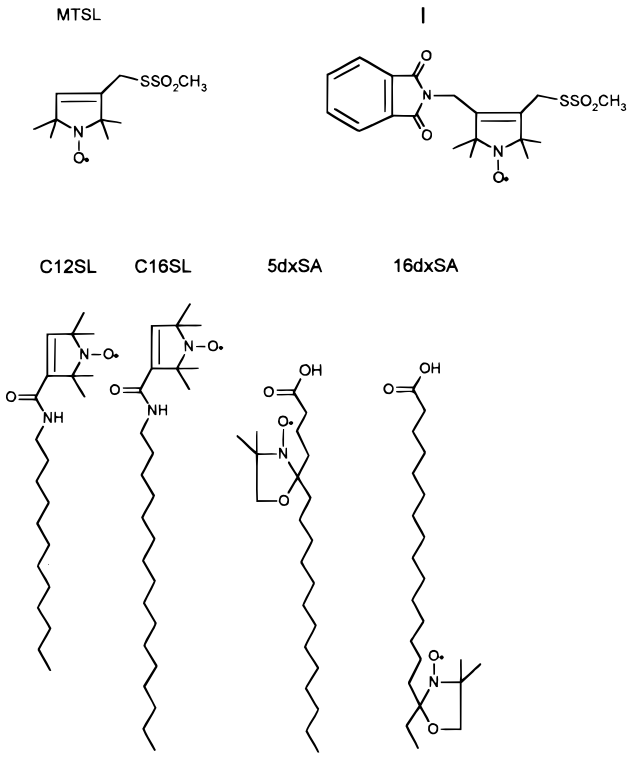

FIGURE 1: Chemical structures of spin-label reagents.

mutant cDNAs were constructed in which corresponding amino acids 95−105 in the G strand of tear lipocalin were converted sequentially to cysteine. Amino acid 95 corresponds to aspartic acid, bases 397−399 of Redl (*6*).

Expression and Purification of Mutant Proteins. The mutant plasmids were transformed in *E. coli*; BL21(DE3) cells were cultured, and the protein was expressed according to the manufacturer's protocol (Novagene). Following cell lysis as previously described (*19*), the supernatant was treated with methanol (final concentration of 40%) and incubated at 4 °C for 2.5 h. The suspension was centrifuged at 3000*g* for 30 min. The supernatant was dialyzed against 50 mM Tris-HCl (pH 8.4). The dialysate was treated with ammonium sulfate at 45−75% saturation. The resulting precipitate was dissolved in 50 mM Tris-HCl (pH 8.4) and applied to a Sephadex G-100 column (2.5 cm × 100 cm) previously equilibrated with 50 mM Tris-HCl and 100 mM NaCl (pH 8.4). The elution profiles of mutant proteins were compared to those of TL-WT and standards, including bovine serum albumin (68 000 Da), carbonic anhydrase (29 000 Da), and egg white lysozyme (14 500 Da). The fractions containing the 35−36 kDa mutant proteins were dialyzed against 50 mM Tris-HCl (pH 8.4) and applied to a DEAE-Sephadex A-25 column. Bound protein was eluted with a 0 to 0.8 M NaCl gradient. Eluted fractions containing mutant proteins were centrifugally concentrated (Amicon, Centricon-10). The purity of mutant proteins was verified by SDS tricine gel electrophoresis (*12*). The protein concentration was determined by the biuret method (*20*).

Spin Labeling of TL Mutants. Mutant and wild-type tear lipocalins (100 μM) were incubated in a 5-fold molar excess of MTSL overnight at 4 °C. Unreacted spin-labels were removed with a HiTrap column. For experiments using the MTSL derivative (**I**), F99C was incubated in a 10-fold molar excess of **I**.

[1] Abbreviations: 5dxSA, 5-doxyl stearic acid; 16dxSA, 16-doxyl stearic acid; CD, circular dichroism; DPPH, 2,2-diphenyl-1-picrylhydrazyl (standard for EPR measurements); DTT, dithiothreitol; EPR, electron paramagnetic resonance; C12SL, spin-labeled analogue of lauric acid; C16SL, spin-labeled analogue of palmitic acid; MTSL, 1,1-oxyl-2,3,5,5-tetramethyl-Δ^3-pyrroline-3-methyl methanethiosulfonate; NiEDDA, nickel(II) ethylenediaminediacetic acid; PAGE, polyacrylamide gel electrophoresis; PCR, polymerase chain reaction; SDSL, site-directed spin labeling; SL, spin-label; TL, tear lipocalin(s); WT, wild-type; WTT, wild-type template.

Circular Dichroic Spectral Measurements. Spectra were recorded (Jasco 600 spectropolarimeter, 0.2 and 10 mm path lengths for far- and near-UV spectra, respectively) using protein concentrations of 1.2 mg/mL. Eight scans were performed from 190 to 260 nm; 16 scans were performed from 250 to 320 nm. Results were recorded in millidegrees.

EPR Measurements. Electron paramagnetic resonance spectra were recorded at X-band with a Varian E-109 spectrometer fitted with a two-loop one-gap resonator (*21*). Samples were loaded in gas-permeable TPX capillaries. The incident microwave power was 2 and 0.05 mW at room temperature and −56 °C, respectively. The modulation amplitude was 1 G.

To characterize accessibility for each protein, power saturation data were obtained under several conditions: under nitrogen gas, under air (20% oxygen), and in the presence of 5 mM NiEDDA under nitrogen gas. Power saturation curves were measured as the vertical peak-to-peak amplitude (A) of the first derivative $M_i = 0$ line as a function of incident microwave power (P) in the range of 0.1−36 mW. The resulting data were fitted to the function

$$A = IP_{1/2}[1 + (2^{1/\epsilon} - 1)P/P_{1/2}]^{-\epsilon}$$

where I is a scaling factor, $P_{1/2}$ is the microwave power at which the observed intensity of the first-derivative center line is half that which would be observed in the absence of saturation, and ϵ is a homogeneity factor. From these data, $\Delta P_{1/2}$ values were calculated by subtracting the $P_{1/2}$ value in the absence of a paramagnetic reagent, $P_{1/2}^{\circ}$ (under nitrogen gas), from the $P_{1/2}$ value in the presence of a paramagnetic reagent (O_2 or NiEDDA); the collision rate with a fast-relaxing paramagnetic reagent is proportional to the change in $P_{1/2}$

$$\Delta P_{1/2} = P_{1/2} - P_{1/2}^{\circ} \propto \omega/T_{2e} \quad (1)$$

where ω is the collision frequency and T_{2e} is the spin−spin relaxation time of the nitroxide (*22*).

Since the peak-to-peak first-derivative line width, ΔH, is proportional to $1/T_{2e}$, $\Delta P_{1/2}$ can be expressed as

$$\Delta P_{1/2}' = \Delta P_{1/2}/\Delta H \propto \omega$$

The accessibility parameter (Π) for spin-labeled TL was calculated using the equation

$$\Pi = \Delta P_{1/2}'/[P_{1/2}(\mathrm{DPPH})/\Delta H(\mathrm{DPPH})]$$

To define an accessibility parameter (Π_a) for spin-labeled fatty acids that is quantitated as a percentage of total accessibility and is independent of the quality factor (Q factor) of the resonator as well as the concentration of the paramagnetic reagent, we determined $\Delta P_{1/2}'$ for the free (completely accessible) C-12 spin-label and compared this to the $\Delta P_{1/2}'$ for the same paramagnetic reagent with the fatty acid spin-label bound to the protein

$$\Pi_a = \frac{\Delta P_{1/2}'(\text{bound ligand})}{\Delta P_{1/2}'(\text{free ligand})} \times 100$$

The diffusion of ligand bound to protein is negligible, and the value of $P_{1/2}'$ of the free ligand reflects the diffusion of both the free ligand and the NiEDDA. Therefore, the accessibility parameter, Π_a, calculated for the accessibility of NiEDDA for spin-labeled fatty acids bound to protein is underestimated by a factor

$$k = [D_{\text{free ligand}} + D_{\text{NiEDDA}}]/D_{\text{NiEDDA}}$$

where D is the diffusion constant of the indicated compound. In the case of oxygen, this factor is not necessary because the diffusion constant of the free ligand is negligible compared to the diffusion constant of oxygen.

To evaluate accessibility where immobile and mobile populations of spin-labeled side chains were resolved, EPR spectra were compared with and without 350 mM $K_3Fe(CN)_6$ (final concentration). For comparison, EPR spectra were normalized for the same number of spins.

Oligomerization of TL. To evaluate the oligomeric state of TL under conditions similar to tears, 1 μL of mutant F99C labeled with the MTSL derivative (**I**) in 10 mM NaP was added to 9 μL of human tears (final F99C concentration of 30 μM and final TL concentration of 67 μM). The resulting dilution of tear components was within the range of normal concentrations (*23*, *24*). The correlation time, τ_R, was calculated from the measurement of the separation between outer hyperfine signals, $2A_{zz}$, at room temperature and in the frozen state, $2A_{zz}'$, according to the following equation (*25*)

$$\tau_R = a(1 - S)^b$$

where $a = 5.4 \times 10^{-10}$, $b = -1.36$, and $S = A_{zz}/A_{zz}'$.

RESULTS AND DISCUSSION

Characterization of Mutant Proteins. The oligomeric complexes of G strand mutants were examined by size exclusion chromatography. The elution profiles of all mutant proteins exhibited a peak at nearly identical volumes as the wild-type TL, consistent with a protein mass of about 35 kDa indicative of a dimer.

To assess the effects of the mutations on secondary structural content, the mutant proteins were characterized with far-UV circular dichroism. Figure 2 shows the CD spectrum of the WTT and WT-TL superimposed over those of the mutants. The CD spectra of all the mutants exhibit a minimum at 214 nm consistent with a β-sheet conformation. Minor distortions are evident with I98C (Figure 2A). The crossover is shifted below 200 nm, and the minimum is 205 nm. These changes may be attributed to changes in packing of secondary structural elements (*26*).

Comparison of the near-UV spectra shows that most of the mutant proteins are quite similar to the WT protein and WTT (Figure 3). It is apparent that the replacement of the aromatic residue tyrosine with cysteine (Y97C) was accompanied by only a slight decrease in the optical activity in the aromatic region compared to that in the WT. In contrast, I98C, H96C, F99C, G103C, and L105C exhibit less optical activity in the aromatic region. In particular, I98C and H96C exhibit markedly less optical activity than the wild type at 285−290 nm, the region of the spectrum contributed predominantly by tryptophan residues (Figure 3A). There is a change in the environment of the aromatic residues (five tyrosines, three phenylalanines, and one tryptophan), i.e., less aromatic side chain rigidity in these mutants than in the WT

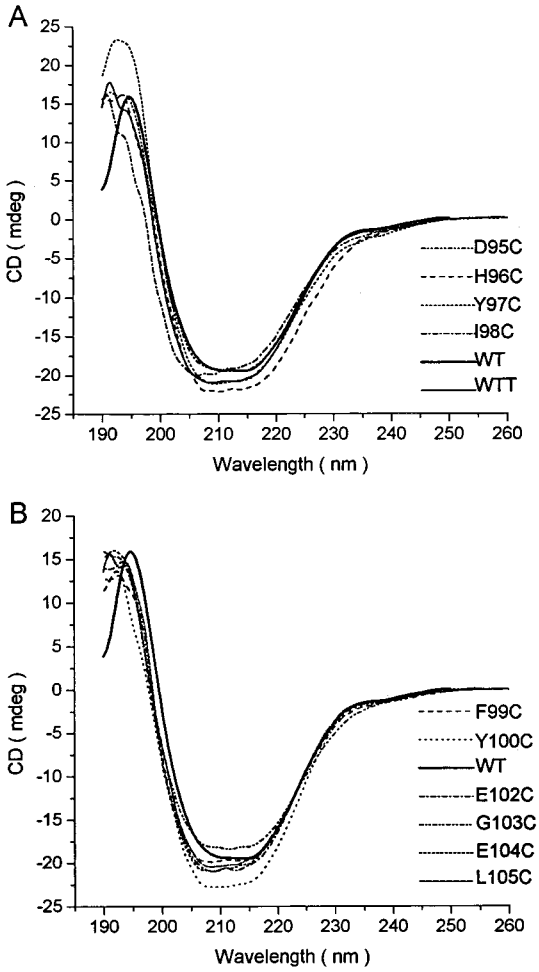

FIGURE 2: Far-UV CD spectra of WTT, WT-TL, and its mutant proteins.

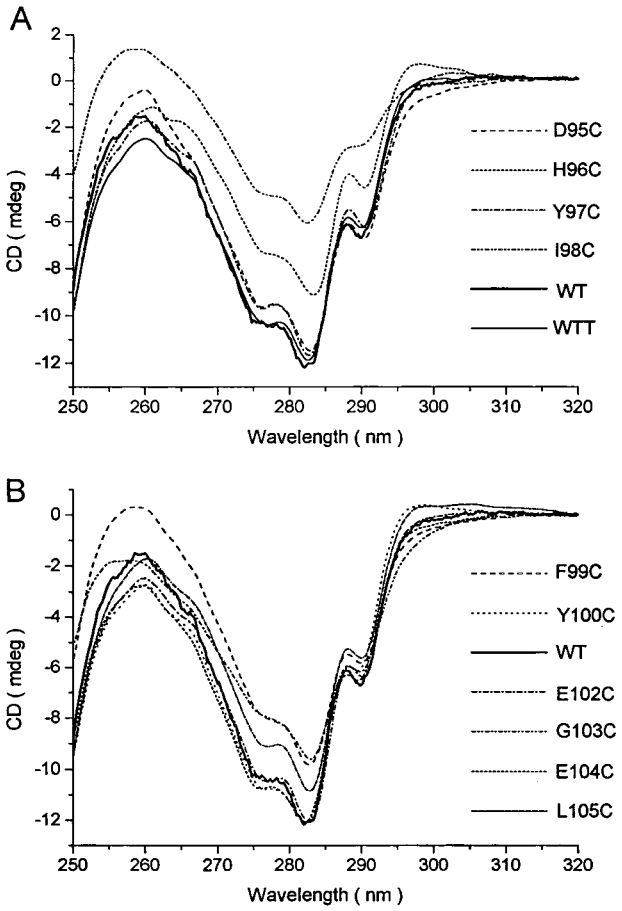

FIGURE 3: Near-UV CD spectra of WTT, WT-TL, and its mutant proteins.

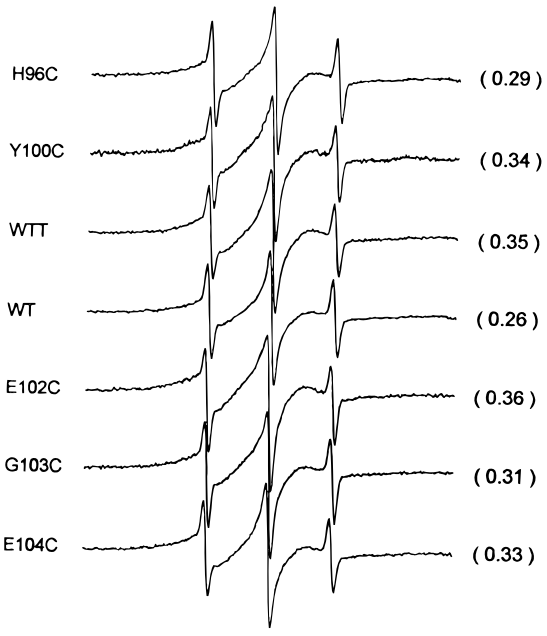

FIGURE 4: EPR spectra of C12SL with WTT, WT-TL, and representative mutants. The numbers in parentheses indicate the ratio of bound to free spin-label signal intensity as estimated by the height of the respective broad and narrow signals in the composite spectra.

even though aromatic amino acids were not replaced. Because the differences in the spectra of the mutants extend to 290 nm, a region affected only by tryptophan, the environment of the single tryptophan on the A strand must be altered. With the exception of I98C, there is no significant change observed in the far-UV CD spectra for the nonaromatic substitutions, indicating that the near-UV spectra changes are not due to secondary structural changes or partial unfolding. Direct contact between the A strand and G strand is quite plausible because in β-lactoglobulin the distances between tryptophan 19 (analogous to tryptophan 17 in TL) and G strand residues tyrosine 102 and leucine 103 are 3.3 and 3.7 Å, respectively (PDB entry 1B0O for β-lactoglobulin).

The fact that mutant proteins retain lipid binding properties was established by the EPR spectra generated when mutant proteins were combined with the spin-labeled analogue of lauric acid. All of the spectra are composites consisting of bound and free components. Figure 4 shows examples of several mutants as well as WTT. The spectra are broadened, indicative of a significant proportion of bound ligand; WTT, WT, and all mutants retained the fundamental property of lipid binding.

Side Chain Mobility along the Sequence of the G Strand. The motion of a nitroxide side chain is reflected in the EPR spectral line shape and is related to the rotational correlation time for the entire protein, the rotational isomerization correlation time about bonds linking the nitroxide to the backbone, and the correlation time for segmental backbone motion relative to the average protein structure. The rotational

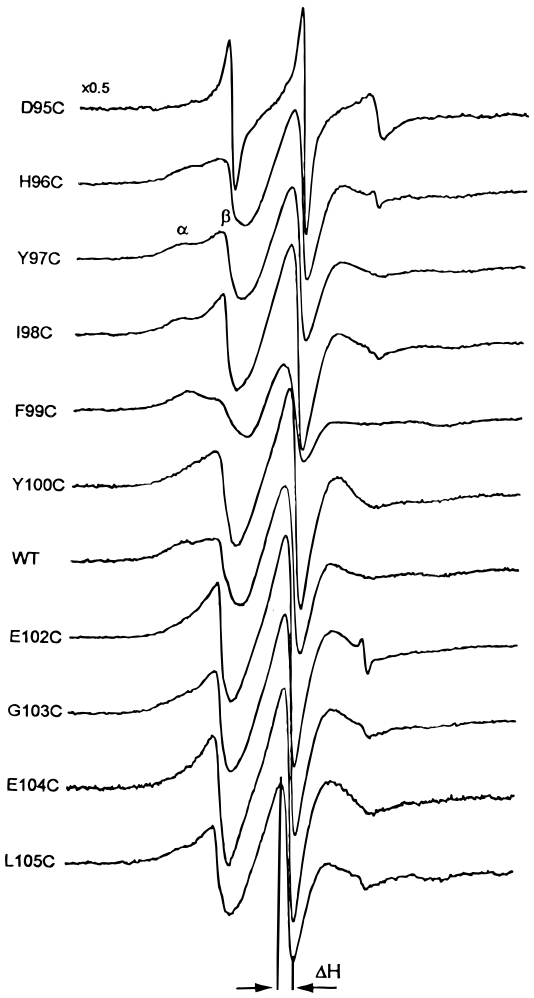

FIGURE 5: EPR spectra of spin-labeled WT-TL and its mutants at room temperature. The spectra were normalized to represent the same number of spins. All spectra were recorded with a 100 G scan width. α and β represent the motionally restricted and mobile components, respectively. The line width of the central resonance, ΔH, is denoted by the arrows.

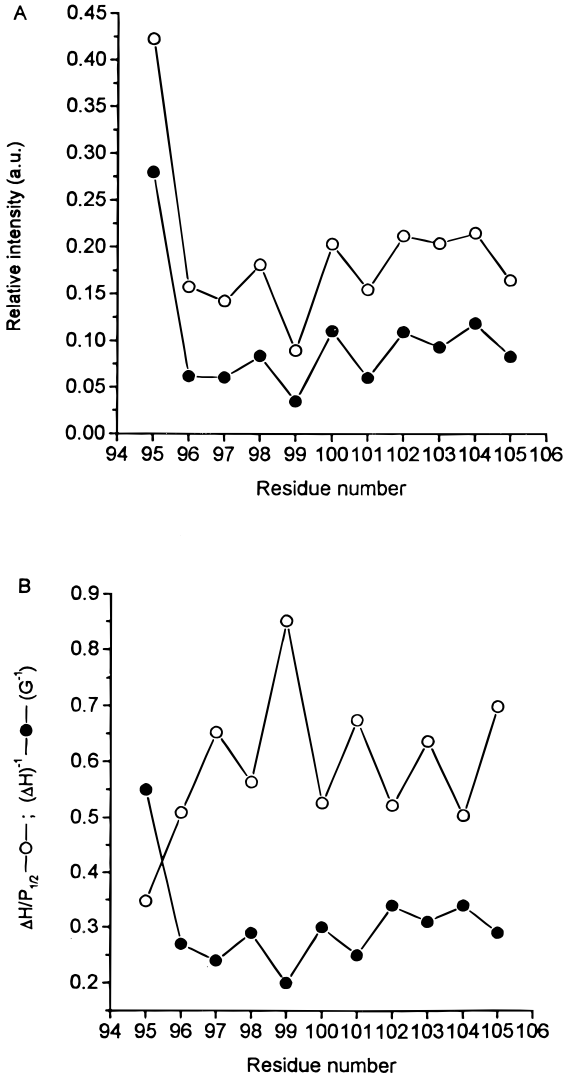

FIGURE 6: (A) Relative intensity of low-field lines (●) and central lines (○) in normalized spectra of WT-TL and its mutants vs residue number. (B) Reciprocal of the central line width ΔH^{-1} (●) and parameter $\Delta H/P_{1/2}$ (○) vs residue number.

mobility of the side chain is dependent on protein structure and on the type of spin-label. The correlation time for segmental motion is determined by the flexibility of the backbone. From inspection of EPR spectra, it is possible to gain a rough assessment of side chain mobility. The overall breadth of the spectrum, the variation of spectral intensity, and the line width of central resonance (ΔH) all reflect mobility (*27*). The EPR spectra of all spin-labeled cysteine mutants are shown in Figure 5. All spectra were normalized to represent the same number of spins. The variation in the spectral intensity of mutants is due predominantly to alteration of side chain mobility. It is evident from inspection that the spectrum of D95C exhibits greater intensity and a narrower line width of the central resonance than those of the other mutants. These changes reflect the greater mobility of the nitroxide. The spectrum shows a complete absence of the motionally restricted component, consistent with an exposed loop region without significant tertiary interactions. ΔH for F99C appears to be relatively broadened, reflecting lower side chain mobility as well as the most motionally restricted component (Figure 5). Further, plots of the parameters of spectral intensity (Figure 6A) and ΔH^{-1} (Figure 6B) versus residue number along the backbone structure of TL reveal alternating periodicity of residues 98−105. ΔH^{-1} is proportional to the spin−spin relaxation time, while the parameter $\Delta H/P_{1/2}$ is proportional to the spin−lattice relaxation time. It is evident in Figure 6 that alternating periodicity exists for residues 98−105 for both parameters. Residues with mobile side chains alternate with motionally constrained residues, a feature that is characteristic of β-structure. These results are consistent with the data obtained by site-directed tryptophan fluorescence of the G strand in TL (*16*). The even-numbered residues are exposed on the external surface of the protein. Odd-numbered residues face the interior of the cavity.

One of the features of the spectra (Figure 5) is the presence in some mutants of two clearly identifiable populations differing in the mobility of the nitroxide side chain relative to the protein. Resolution of these two populations is evident in Y97C and I98C. The contribution of the motionally restricted component, α, varies in the different spectra (Figure 5). Alternating periodicity exists such that the odd-numbered mutants along the chain exhibit a greater contribution of the immobile component than the nearest numbered neighbor; e.g., I98C exhibits a larger mobile component, β, than either

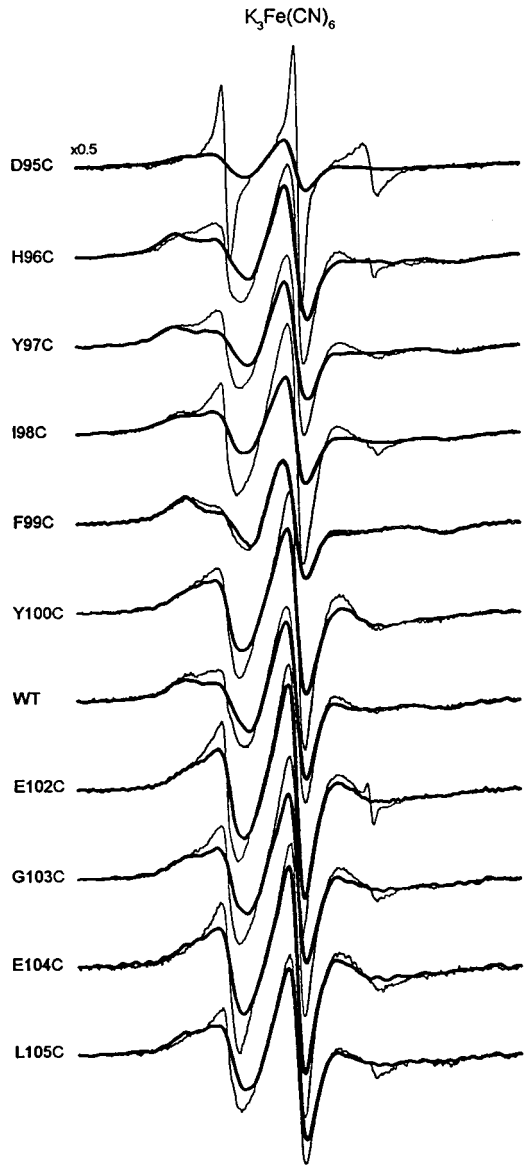

FIGURE 7: EPR spectra of WT-TL and its mutant proteins in buffer (thin lines) and 350 mM $K_3Fe(CN)_6$ (thick lines).

F99C or Y97C. The differences are evident but quite subtle for E102C through L105C. These features are comparable to the alternating periodicity observed with other parameters of mobility (Figures 5 and 6). The spectrum of WT-TL demonstrates the resolution of the mobile and relatively motionally restricted nitroxide spin-labeled side chain populations. The resolution of these populations is enhanced with a fast relaxing reagent such as $K_3Fe(CN)_6$ which reduces spin−spin and spin−lattice relaxation times (Figure 7). With suitable concentrations of $K_3Fe(CN)_6$, the influence on the spin−spin relaxation time results in a broadening of the spectrum and a decrease in intensity for accessible nitroxide-labeled residues (e.g., D95C). In contrast, F99C exhibits only a subtle change in its spectral characteristics with $K_3Fe(CN)_6$. Because the spin−spin relaxation time ($T_2 \sim 10^{-8}$ s) is much shorter than the spin−lattice relaxation time ($T_1 \sim 10^{-6}$ s), changes in T_2 may be observed only with concentrations of fast-relaxing reagents that are 100-fold greater than the concentration that is necessary for studying the accessibility parameter that is dependent on T_1. This phenomenon is evident in Figure 7. The concentration of $K_3Fe(CN)_6$ will

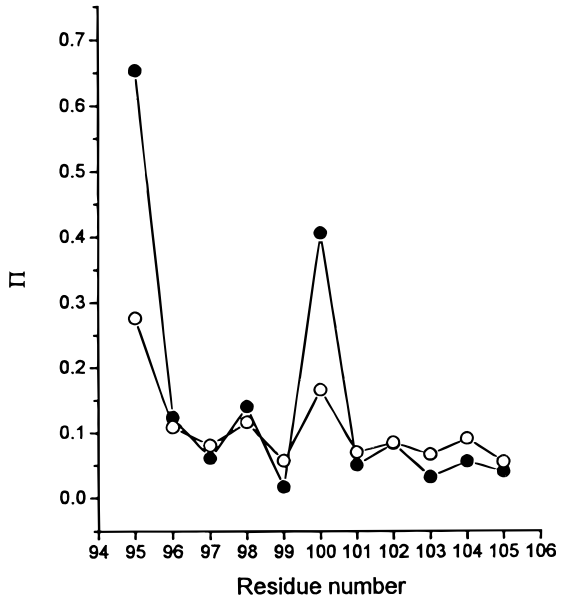

FIGURE 8: Accessibility parameters Π(NiEDDA) (●) and Π(O_2) (○) vs residue number of WT-TL and mutant proteins.

influence the mobile and immobile components differently according to both the accessibility of the spin-label and the line width of the central resonance. Because the EPR signal intensity varies with the inverse square of the line width of the central resonance, the equivalent changes in line width influence intensity much more in the spectra with the narrower initial line width. Hence, $K_3Fe(CN)_6$ aids in distinguishing two populations by broadening and lowering the intensity of the EPR signal more in the mobile population than in the immobile population. In Figure 7, for H96C, Y97C, I98C, and TL-WT in $K_3Fe(CN)_6$, the intensities of the mobile components of each spectrum are markedly reduced and the line shapes broadened. There is less of an effect on the motionally restricted components of each spectrum. The changes in other mutants are present but less apparent. The clarification of the mobile and immobile components in $K_3Fe(CN)_6$ by reduction of the more mobile population demonstrates side chain interaction (tertiary contact) of the motionally restricted component. The tertiary contact is likely to result from side chain interaction of an adjacent strand rather than nearest-neighbor interactions of the same strand (*28*). Amino acid residue 98 is oriented toward the solvent and provides the best resolution of tertiary contact. The perturbation of secondary structure in I98C (decreased optical activity at 215 nm and formation of a spectral minimum at 205 nm) is related to packing and differences in aromatic side chain rigidity (*26*). The tertiary interactions of side chains in I98C appear to be more sensitive to perturbations than other residues.

Accessibility Profile in NiEDDA and O_2. The accessibility parameter, Π, is a measure of the extent of solvent exposure of a side chain. It is determined from the change in parameter $P_{1/2}$, in the presence of NiEDDA or 20% oxygen (air). Figure 8 shows the sequence-specific variation in Π. It is evident that D95C is very accessible to both oxygen and NiEDDA. In contrast, F99C is relatively inaccessible compared to other residues in the G strand. From residue 98 to 105, there is alternating periodicity of accessibility similar to what was observed with the mobility parameters and EPR spectral line shapes (Figures 5 and 6). These features delineate the

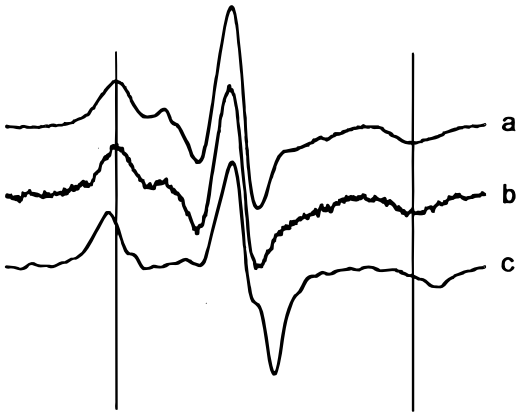

FIGURE 9: EPR spectra of F99C with the spin-label (**I**) in 10 mM sodium phosphate (pH 7.3) (a), in tears (b), and in the frozen state in buffer (c).

residues involved in the formation of the β-strand. The accessibility at residue Y100C is greater than that of the other residues. There are a number of possible explanations, including the possibility that side chain residues adjacent to residue 100 are smaller than the adjacent side chains of the other residues on the external surface of the G strand.

Dimeric State of TL. To investigate the oligomeric state of TL under conditions approaching those in tears, we labeled the most motionally restricted of the side chain residues, F99C, with an MTSL derivative (**I**, Figure 1). The bulky structure of this derivative (**I**) resulted in a lack of rotational motion about the side chain. Therefore, the rotation of the spin-label reflects the rotation of the entire protein and its correlation time. The expected correlation time for dimeric TL is about 13 ns; for monomeric TL, it is about 6.5 ns. It is evident that the correlation time for F99C in buffer is the same as in tears or 13.5 ns (Figure 9). It is plausible to conclude that TL exist in dimeric form in tears. It is known that TL exist largely as noncovalent dimers in fractions eluted from column chromatography (*6*, *14*). Other lipocalins, including odorant binding protein, major urinary protein, β-lactoglobulin, and α_2-microglobulin, have been purified in dimeric form and are believed to exist in the native states as dimers (*2*, *29*). In crystallographic studies of β-lactoglobulin, the dimer is formed through the association of the I strands (*7*). The dimer formed in this way does not permit interaction of the mouths of the calyces; ligands bind independently to each subunit. The stoichiometry of binding for TL is 1:1, consistent with a ligand interaction like that of β-lactoglobulin.

Ligand Orientation and Accessibility in the Cavity of TL. To study ligand orientation and accessibility within the cavity of TL, we employed a series of fatty acid derivative ligands with nitroxides positioned at different points along the hydrocarbon chain. The broadened spectra generated from TL incubated with these ligands demonstrate the presence of a spin-label that is protein-bound (Figure 10). All of the ligands exhibit greater accessibility to oxygen than NiEDDA, consistent with a position within the TL cavity rather than at the surface (Figure 11). In addition, it is evident from a comparison of the spectrum of F99C (Figure 9) to the spectra of SL ligands bound to TL (Figure 10) that the correlation time of the SL ligand in the bound state is smaller than that of the SL protein. Hence, there is additional movement that can be attributed to segmental motion of ligands in the cavity.

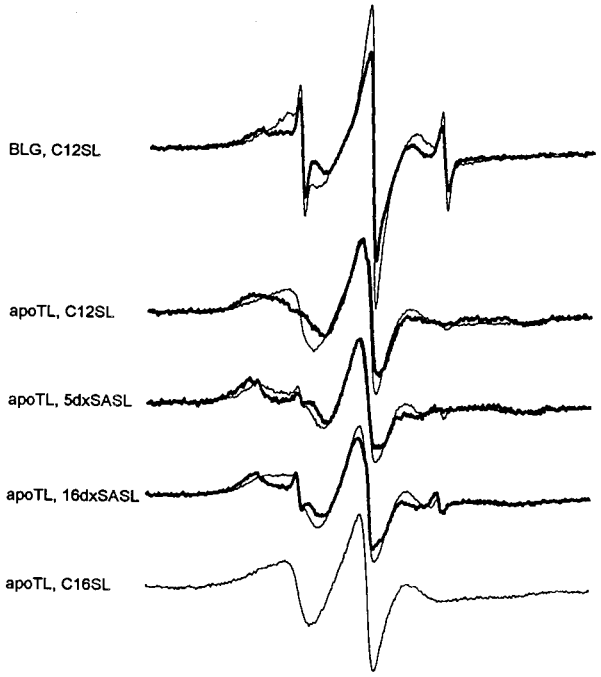

FIGURE 10: EPR spectra of C12SL (60 μM) incubated with β-lactoglobulin (50 μM) as well as spectra of various spin-labeled ligands (50 μM) and apo-TL (200 μM). Thick and thin lines represent spectra recorded in 10 mM sodium phosphate (pH 7.3) with and without 30% sucrose, respectively. Protein concentrations were chosen with a molar excess of apo-TL to yield only the bound form of the ligand. For β-lactoglobulin, the free spectrum of C12SL was subtracted from the composite spectrum of bound and free to give the pure bound spectrum.

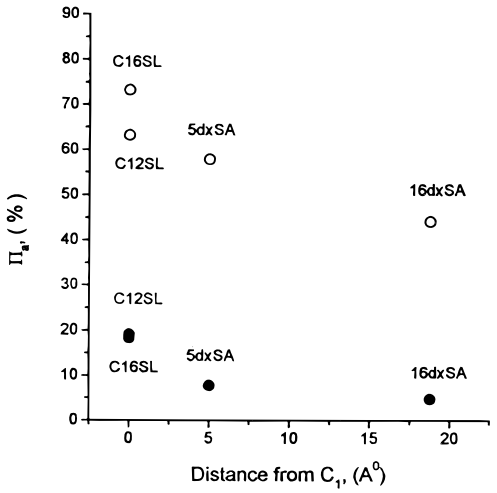

FIGURE 11: Percentage of accessibility Π_a(NiEDDA) (●) and Π_a-(O_2) (○) at various distances between the nitroxide and the first carbon atom (C_1) of the indicated ligand. When the nitroxide group is attached to the first carbon, the distance was taken to be 0 Å.

It is also evident from Figure 10 that the correlation time of SL bound to β-lactoglobulin is smaller than the correlation time of β-lactoglobulin without an attached ligand (about 13 ns). Therefore, for both TL and β-lactoglobulin, the ligands are not rigidly held in the cavity but rather exhibit segmental motion.

Analysis of the EPR spectra reveals the orientation of the ligands in the lipocalin cavity. The lauric and palmitic acid analogues have the nitroxide positioned adjacent to the carbonyl group. When these analogues are bound to TL, the nitroxides are highly mobile. In contrast, 5dxSA and 16dxSA

exhibit markedly less mobility of the nitroxide in the bound state. 16dxSA has lower accessibility to both oxygen and NiEDDA but is more mobile than 5dxSA. The accessibility parameters (Figure 11) of 5dxSA and 16dxSA are smaller than those of the spin-labeled derivatives of lauric and palmitic acid for both NiEDDA and oxygen. 16dxSA with the nitroxide positioned closest to the hydrocarbon tail is the least accessible; therefore, the hydrocarbon tail must be buried deep in the cavity and the carboxyl side chain is located more superficially. The nitroxide side chains in the lauric and palmitic acid derivatives are mobile and have greater accessibility than the stearic acid derivatives. Hence, the more mobile nitroxides adjacent to the carbonyl group are oriented more superficially, and the hydrocarbon tail is oriented deep in the cavity. These data are consistent with our previously published conclusions regarding the orientation of the C12SL (*12*). In the case of the palmitic acid derivative, the nitroxide is oriented toward the mouth and motionally restricted, and thus clearly enveloped within the cavity. Therefore, the TL cavity has the capacity for molecules with at least 16 carbon units. Other lipocalins, such as β-lactoglobulin, can encompass ligands with at least 16 carbon units (*8*). The crystal structure of β-lactoglobulin bound to lauric and palmitic acids revealed that these fatty acids are completely encompassed by the protein with the carboxyl group oriented toward the mouth of the cavity (*8*). Our data indicate that the lauric and palmitic acid derivatives have similar Ni accessibility and slight differences in O_2 accessibility, suggesting the nitroxides lie at a similar depth and are oriented toward the cavity mouth while the hydrocarbon chains extend for different lengths inside the TL cavity. The spectrum for C12SL bound to β-lactoglobulin (Figure 10) indicates less motional restriction than the published spectrum of 5dxSA (*30*). Therefore, β-lactoglobulin and TL are similar in that the nitroxide of bound 5dxSA is oriented deeper in the cavity than in C12SL. However, in contrast to our results with TL, Narayan et al. concluded that 16dxSA does not bind β-lactoglobulin presumably due to steric influences of the nitroxide moiety. These data may suggest that TL is a more promiscuous molecule than β-lactoglobulin.

It is also evident from Figure 10 that nitroxide spin-labels located at the mouth of the cavity (lauric and palmitic acid derivatives) are more mobile than those located deep in the cavity (5dxSA and 16dxSA). Similar conclusions were drawn from X-ray crystallography of β-lactoglobulin (*8*). Palmitate carbons C-8−C-16 within the β-lactoglobulin cavity exhibit fluctuations (*B* factor) similar to that of adjacent amino acid residues, but those palmitate carbons oriented toward the mouth of the cavity exhibit greater fluctuations than the surrounding residues.

Influence of Sucrose on Secondary and Tertiary Structure. The question of whether there is any conformational change in response to the addition of viscogenic agents arises. The effects of increased viscosity on secondary and tertiary structure were investigated by examining the far- and near-UV CD spectra of TL with and without 30% sucrose. As shown in Figure 12, the circular dichroism spectra in buffer are identical to those obtained with the addition of sucrose. The cosolvent does not induce any substantial change in the packing of secondary structural elements or in discernible tertiary structure.

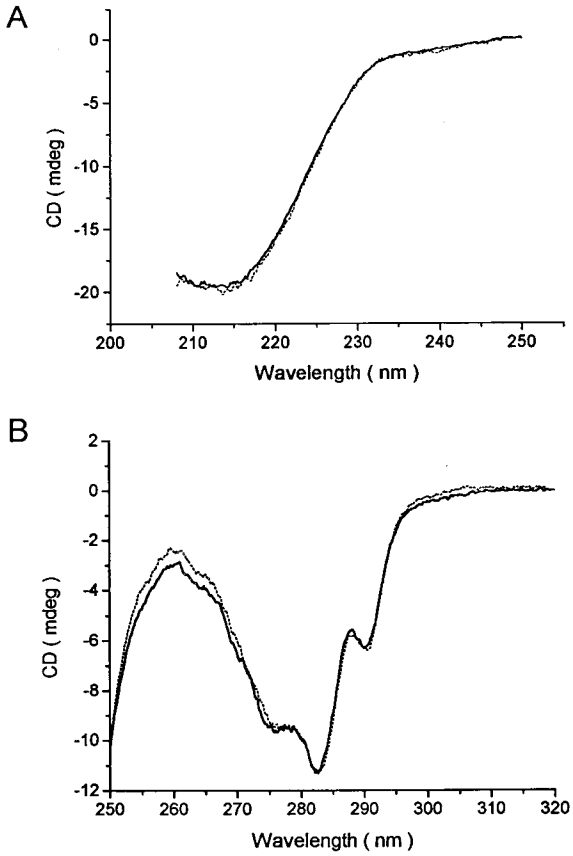

FIGURE 12: Far (A)- and near-UV CD spectra (B) of TL with and without 30% sucrose (dotted and solid lines, respectively).

Influence of Sucrose on Side Chain Mobility and Ligand Binding. The effects of sucrose on side chain mobility and structural fluctuations were investigated with the spin-labeled mutant proteins in 30% sucrose (Figure 13). For all the mutants that are shown, there is decreased side chain mobility reflected by the decreased spectral intensity of the mobile component, a corresponding increase in the immobile component, and the increased line width of the central resonance. In buffer alone, the spectra of residues 103−105 exhibit various contributions from mobile and motionally restricted populations. The nitroxide at residue E104C is more mobile than the one at G103C or L105C. The mobility of all residues is decreased in sucrose. But for residue 104, the decrease is greater such that the mobility of E104C approaches that of G103C and L105C. The solution of 30% sucrose reduces the mobility of E104C, a relatively exposed residue in the β-sheet, more than the adjacent less exposed residues.

In 30% sucrose, residues 102−105 exhibit more narrow spectra than residues 98 and 99. I98C and F99C are both relatively immobile in 30% sucrose, whereas residues 102−105 are less constrained. For motionally restricted nitroxides, the measurement of the separation between outer hyperfine signals, $2A_{zz}$, reflects the polarity of the environment. Hence, we can compare the environment of the two side chain residues I98C and F99C. I98C ($2A_{zz}$ = 68 G) has a broader spectrum than F99C ($2A_{zz}$ = 63 G) in 30% sucrose, suggesting it is surrounded by a more polar environment. The experiments performed in the frozen state (Figure 13) verify that I98C ($2A_{zz}$ = 73.3 G) is in a more polar environment than F99C ($2A_{zz}$ = 68.9 G).

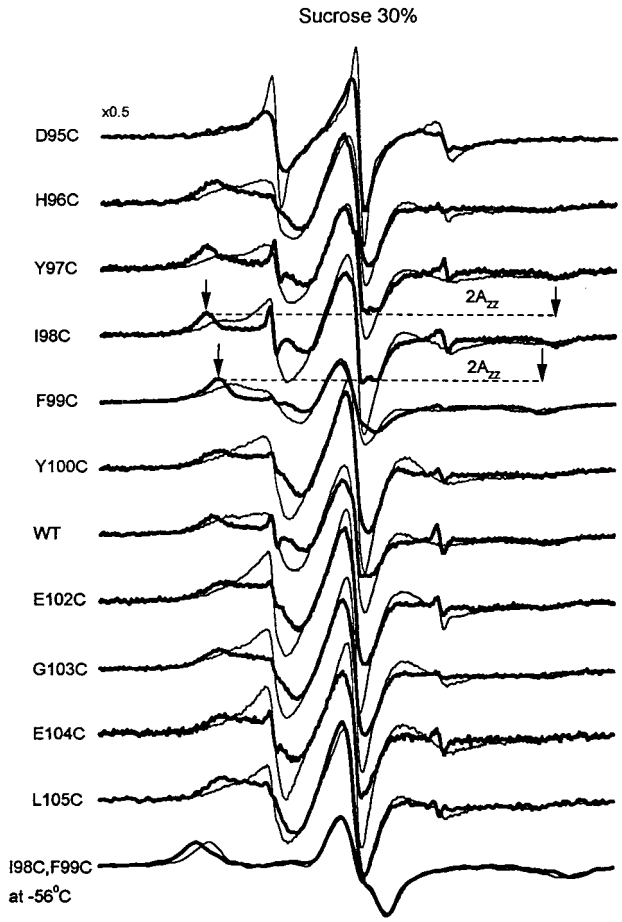

FIGURE 13: EPR spectra of WT-TL and its mutants in 10 mM sodium phosphate (pH 7.3) (thin lines) and in the buffer containing 30% sucrose (thick line). $2A_{zz}$ is the distance between the outer hyperfine signals (arrows). The EPR spectra of I98C and F99C in the frozen state are represented separately with thick lines and thin lines, respectively.

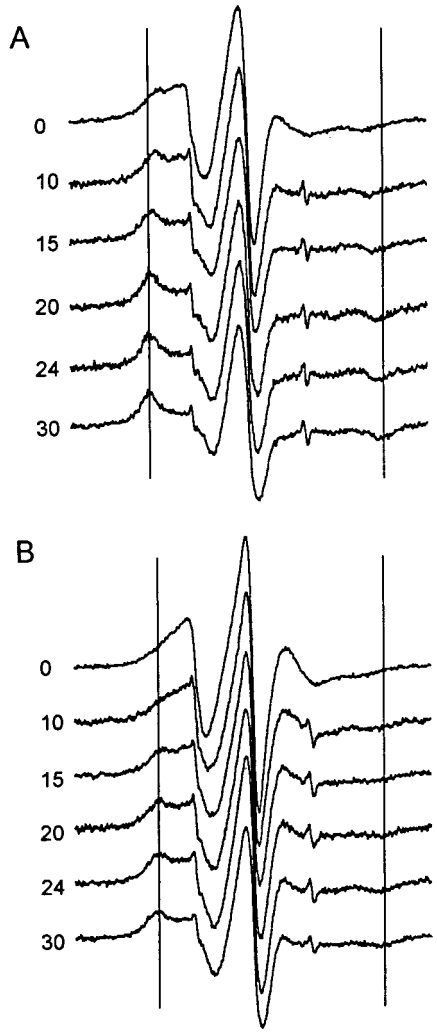

FIGURE 14: EPR spectra of (A) WT-TL and (B) Y100C in various concentrations of sucrose (shown in percentages).

For the side chain residues in which both mobile and relatively immobile populations are observed, it is possible to separate the influence of the rotation of the nitroxide from the effects of backbone fluctuation in solutions containing graded concentrations of sucrose. It is evident that sucrose does not influence a nitroxide in rapid motion, i.e., a free nitroxide (Figures 14 and 15). The effects of increasing viscosity are slowing the overall rotation of the protein and reducing the rate of conformational changes (*31*). Others have argued that the effect of sucrose on backbone motion is independent of viscosity (*32*). In 30% sucrose, the rotation of the protein is slowed by a factor of 3 (*26*). The contribution of protein rotation to the line shape becomes negligible compared to the influence of nitroxide motion. For two mutants, Y100C and WT-TL, the widths of the spectra do not increase in solutions of 20−30% sucrose, indicating that the nitroxide-labeled residues are not slowed. Yet, the contribution from the motionally restricted population increases in intensity, suggesting that slowed backbone motion is responsible for an increased population with tertiary contact.

The effects of sucrose on ligand mobility were investigated for C12SL and apo-TL in sucrose (Figure 15). It is evident that 30% sucrose minimally influences free C12SL that is rapidly moving in solution. For TL incubated with C12SL in sucrose (Figure 15b), the composite spectrum exhibits a broader motionally restricted component compared to the spectrum without sucrose (Figure 15a). It is also evident that there is decreased intensity of the mobile component in sucrose. The decreased intensity of the mobile component can be attributed to the greater affinity of TL for C12SL in sucrose. This implies a stronger hydrophobic interaction between ligand and TL is permitted because of the decreased level of backbone fluctuations in sucrose.

Differences in the EPR spectra of spin-labeled analogues in sucrose permit conclusions about the backbone motion of TL. Nitroxide-bearing ligands that are exposed to sucrose are susceptible to a dampening effect on rotational motion. However, those nitroxides on ligands buried in the cavity are not exposed to the effects of sucrose on rotational motion. For buried ligands, changes in EPR spectra reflect changes in the interactions of amino acid residues with the nitroxide spin-labeled ligands. These interactions are probably due to dampening of backbone fluctuations of the protein. From the orientation of the spin-labeled compounds and the lack of accessibility to NiEDDA, it is clear that the nitroxides on all of our ligands are enveloped by the protein and relatively unexposed to sucrose. This is most obvious for 5dxSA and 16dxSA. In each case, the spectrum in sucrose indicates a decreased level of motion of the nitroxide spin-label compared to the spectrum without sucrose (Figures 10 and 11).

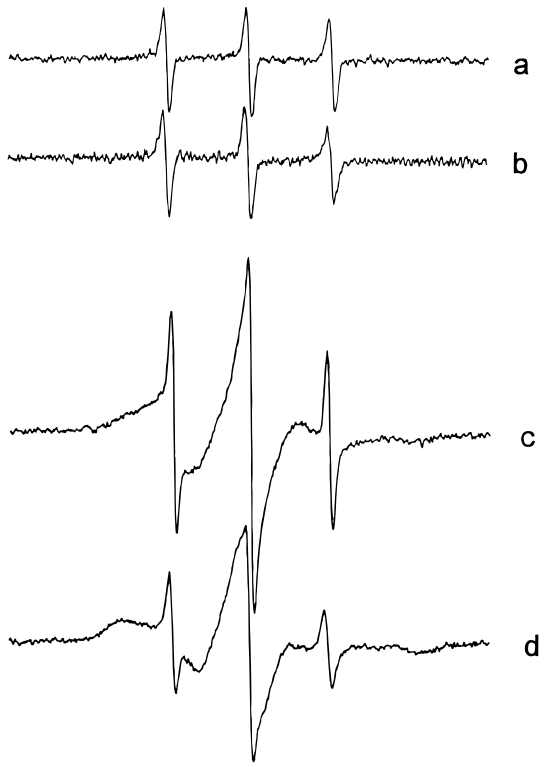

FIGURE 15: EPR spectra of C12SL in 10 mM sodium phosphate (pH 7.3) (a) and in 10 mM sodium phosphate (pH 7.3) and 30% sucrose (b). EPR spectra of C12SL (40 μM) incubated with apo-TL (50 μM) in 10 mM sodium phosphate (pH 7.3) (c) and in 10 mM sodium phosphate (pH 7.3) and 30% sucrose (d).

Because the nitroxide-labeled ligands are located at various depths in the cavity, we attribute the restricted motion in sucrose to a decreased calyx volume. It is apparent that the motion of the spin-label analogue of lauric acid bound to β-lactoglobulin is also reduced in sucrose, indicating a similar influence of backbone motion on ligand interactions (Figure 10). The crystal structure has revealed that lauric acid is also enveloped by β-lactoglobulin. Since our EPR spectra of spin-labeled lauric acid in TL show similar motion in β-lactoglobulin, we conclude that it is enveloped in the calyx and that the backbone motion is responsible for the effects of sucrose. It is clear from these data that the bound state of the ligand is influenced by backbone motion of the lipocalins.

ACKNOWLEDGMENT

Joseph Horwitz provided access to the Jasco 600 spectropolarimeter.

REFERENCES

1. Flower, D. R. (1994) *FEBS Lett. 354*, 7−11.
2. Flower, D. R. (1996) *Biochem. J. 318*, 1−14.
3. Papiz, M. Z., Sawyer, L., Eliopoulos, E. E., North, A. C. T., Findlay, J. B. C., Sivaprasadarao, R., Jones, T. A., Newcomer, M. E., and Kraulis, P. J. (1986) *Nature 324*, 383−385.
4. Molinari, H., Ragona, L., Varani, L., Musco, G., Consonni, R., Zetta, L., and Monaco, H. L. (1996) *FEBS Lett. 381*, 237−243.
5. Monaco, H. L., Zanotti, G., Spadon, P., Bolognesi, M., Sawyer, L., and Eliopoulos, E. E. (1987) *J. Mol. Biol. 197*, 695−706.
6. Redl, B., Holzfeind, P., and Lottspeich, F. (1992) *J. Biol. Chem. 267*, 20282−20287.
7. Qin, B. Y., Bewley, M. C., Creamer, L. K., Baker, H. M., Baker, E. N., and Jameson, G. B. (1998) *Biochemistry 37*, 14014−14023.
8. Wu, S.-Y., Pérez, D., Puyol, P., and Sawyer, L. (1999) *J. Biol. Chem. 274*, 170−174.
9. Narayan, M., and Berliner, L. J. (1998) *Protein Sci. 7*, 150−157.
10. Huber, R., Schneider, M., Mayr, I., Müller, R., Deutzmann, R., Suter, F., Zuber, H., Falk, H., and Kayser, H. (1987) *J. Mol. Biol. 198*, 499−513.
11. Holden, H. M., Rypniewski, W. R., Law, J. H., and Rayment, I. (1987) *EMBO J. 6*, 1565−1570.
12. Glasgow, B. J., Abduragimov, A. R., Farahbakash, Z., Faull, K. F., and Hubbell, W. L. (1995) *Curr. Eye Res. 14*, 363−372.
13. Fullard, R. J., and Kissner, D. M. (1991) *Curr. Eye Res. 10*, 613−628.
14. Glasgow, B. J., Abduragimov, A. R., Yusifov, T. N., Gasymov, O. K., Horwitz, J., Hubbell, W. L., and Faull, K. F. (1998) *Biochemistry 37*, 2215−2225.
15. Gasymov, O. K., Abduragimov, A. R., Yusifov, T. N., and Glasgow, B. J. (1998) *Biochim. Biophys. Acta 1386*, 145−156.
16. Gasymov, O. K., Abduragimov, A. R., Yusifov, T. N., and Glasgow, B. J. (1997) *Biochem. Biophys. Res. Commun. 239*, 191−196.
17. Hubbell, W. L., and McConnell, H. M. (1971) *J. Am. Chem. Soc. 93*, 314−325.
18. Glasgow, B. J., Heinzmann, C., Kojis, T., Sparkes, R., Mohandas, T., and Bateman, J. B. (1993) *Curr. Eye Res. 11*, 1019−1023.
19. Marston, F. A. O. (1987) in *DNA Cloning, Volume III, A Practical Approach* (Glover, D. M., Ed.) p 62, IRL Press, Oxford, England.
20. Bozimowski, D., Artiss, J. D., and Zak, B. (1985) *J. Clin. Chem. Clin. Biochem. 23*, 683−689.
21. Hubbell, W. L., Froncisz, W., and Hyde, J. S. (1987) *Rev. Sci. Instrum. 58*, 1879−1997.
22. Farhbakhsh, Z. T., Altenbach, C., and Hubbell, W. L. (1992) *Photochem. Photobiol. 56*, 1019−1033.
23. Fullard, R. J., and Tucker, D. L. (1991) *Invest. Ophthalmol. Visual Sci. 32*, 2290−2301.
24. Von Haeringen, N. J. (1980) *Surv. Ophthalmol. 28*, 84−96.
25. Freed, J. H. (1976) in *Spin Labeling, Theory and Applications* (Berliner, L. J., Ed.) pp 53−132, Academic Press, New York.
26. Berengian, A. R., Bova, M. P., and Mchaourab, H. S. (1997) *Biochemistry 36*, 9951−9957.
27. Mchaourab, H. S., Lietzow, M. A., Hideg, K., and Hubbell, W. L. (1996) *Biochemistry 35*, 7692−7704.
28. Hubbell, W. L., Gross, A., Langen, R., and Leitzow, M. A. (1998) *Curr. Opin. Struct. Biol. 8*, 649−656.
29. Bianchet, M. A., Bains, B., Pelsi, P., Pevner, J., Snyder, S. H., Monaco, H. L., and Amzel, L. M. (1996) *Nat. Struct. Biol. 3*, 934−939.
30. Narayan, N., and Berliner, L. J. (1997) *Biochemistry 36*, 1906−1911.
31. Ansari, A., Jones, C. M., Henry, E. R., Hofrichter, J., and Eaton, W. A. (1992) *Science 256*, 1796−1798.
32. Butler, S. L., and Falke, J. J. (1996) *Biochemistry 35*, 10595−10600.

BI9913449